Prediction of Forming Forces for Incremental Micro-Forming Using Finite Element Analysis

Submitted: 2021-12-09

Revised: 2022-02-08

Online: 2022-07-22

Accepted: 2022-02-08

Ankush Bansal^{1,a}, Randy Cheng^{2,b}, Mihaela Banu^{1,c}, Alan Taub^{1,2,d} and Jun Ni^{1,e}

¹Department of Mechanical Engineering, University of Michigan, Ann Arbor, USA

²Department of Material Science and Engineering, University of Michigan, Ann Arbor, USA

^aankb@umich.edu, ^brandyjfc@umich.edu, ^cmbanu@umich.edu, ^dalantaub@umich.edu,

^ejunni@umich.edu

Keywords: Microforming, finite element analysis, incremental forming, Al 1100

Abstract. As incremental forming is a relatively new sheet metal forming process, very limited analytical and finite element prediction models are available in literature to study the process mechanics and improve its performance. Thus, most studies involve many trial-and-error iterations to optimize the processing conditions in order to take advantage of high process flexibility and material formability. However, reducing efforts of trial-and-error iterations is of utmost importance to make a process financially viable. Therefore, an FE model is developed and experimentally validated to predict the forming forces involved in incremental micro-forming process. Different mass scaling factors and element-types are used to optimize and develop the model for accurate prediction in the least possible computation time.

Introduction

Product miniaturization is becoming increasingly important because of their widespread applications in biosensors, bio-scaffolds and micro-electronics systems. To meet this increasing market demand, fabrication of micro/meso-scale products through various forming processes such as precision-milling, micro-EDM, micro-deep drawing, micro-punching, micro-blanking and micro-coining have been extensively studied in recent years [1]. Lately, micro-additive manufacturing and direct laser writing (DLW) are also gaining attention for low-volume or personalized production of biocompatible parts and scaffolds from stem cell growth [2].

In this article, a rapid manufacturing technique called incremental sheet micro-forming (µISF) used for producing three-dimensional structures of metallic foils is experimentally and numerically investigated. The process was first introduced by Saotome and Okamoto [3] in 2001. They formed a 600 µm long car body-shell through repetitive hammering on a 10 µm thick aluminum foil. Obikawa et al. [4] later developed a table-top CNC machine setup to demonstrate the µISF process capabilities by conducting a comprehensive parametric study and fabricating complex structures using aluminum foils. In subsequent work, Obikawa and Hayashi [5] integrated ultrasonic spindle with axial vibrations to enhance material formability and produce parts of high strength materials such as stainless steel and titanium foils. In addition, they also applied localized laser heating to reduce springback and achieve better geometric accuracy while forming sub-millimeter size parts. However, knowledge from macro-scale part production cannot be directly applied to micro-scale processes due to scaling effects of grain to thickness ratio in sheet metal forming. This scaling effect shows significant influence on sheet springback [6], surface roughness, flow stress and material forming limit [7].

As it is a relatively new micro-forming process, very limited analytical and finite element prediction models are available to study the process mechanics and improve its performance. Thus, most studies involve many trial-and-error iterations to optimize the processing conditions in order to take advantage of the major advantages of high flexibility and material formability with minimal tradeoff on geometric accuracy. However, reducing efforts of trial-and-error iterations is of utmost importance to make a process financially viable by reducing the amount of lead time and material tooling costs. Advances in finite element analysis (FEA) can be used to accurately represent the

complex deformation process and capture local mechanical response of the material under the forming tool. In addition, it will help better understand the process mechanics and complement the further development of analytical process prediction models.

Numerical simulations of macro-scale ISF process are widely utilized to predict its process performance and gain knowledge of underlying mechanics. Some of the key considerations in designing FE models for incremental forming to attain good precision, highlighted by Behera et al. [8], are constitutive material models, choice of integration schemes (explicit or implicit), element type (solid or shell element) and surface interaction modeling. He et al. [55] developed an elastoplastic FE model using implicit Abaqus/Standard package for the simulations of SPIF process. Implicit solver is known to consume high computation time. It showed promising results in explaining plain-strain state of deformation but struggled to achieve good prediction accuracy in forming forces when compared with experimental values. Other FE simulations [9] explained that kinematic hardening models could predict much better part geometries compared to simple isotropic hardening law. Esmaeilpour et al. [10], [11] pointed out that significant out-of-plane shear stress developed in the ISF process requiring implementation of a 3D yield function to accurately represent its complex nature of 3D stress state. They calibrated the Barlat Yld2004-18p non-quadratic yield function using crystal plasticity model as out-of-plane tensile test properties could not be obtained experimentally. The developed FE model was run to simulate the fabrication of cone 45° geometry and validated against experimental results. Predicted axial and radial forces showed great agreement with the experimentally obtained values. Moser et al. [12] performed extensive analysis of ISF simulation by ABAQUS/Explicit solver scheme to study the effect of mass and velocity scaling on prediction results. Using a simple FE model for DSIF process, they demonstrated that changing mass scaling significantly increased the kinetic energy in the system. However, it did not have much influence on the forming forces other than some scattered sporadic values.

Experimental Setup

An experimental setup is developed in-house by assembling three linear stages with point-to-point motion accuracy of 2 μ m as presented by authors in [13]. Force sensor (ATI gamma F/T sensor) is integrated in the setup to record forming forces along x, y and z-directions through the fabrication process. A set of experiments is performed through μ SPIF processing of 50 μ m thick AL 1100 foils. Helical-type toolpath is generated to form the miniature parts of truncated conical geometry with: a. wall angle = 45°, b. opening diameter = 2 mm and c. depth = 0.75 mm as shown in Figure 1. Process parameters are kept constant at: a. step size = 10 μ m, b. tool-tip diameter = 150 μ m and c. feed rate = 2 mm/sec. Once fabricated, the parts are scanned under an optical profilometer, while still clamped in the fixtures, to create a 3D map of its final geometry. From the scanned data, vertical cross-sectional profiles are extracted and compared with designed geometry to quantify its dimensional accuracy along both rolling and transverse directions.

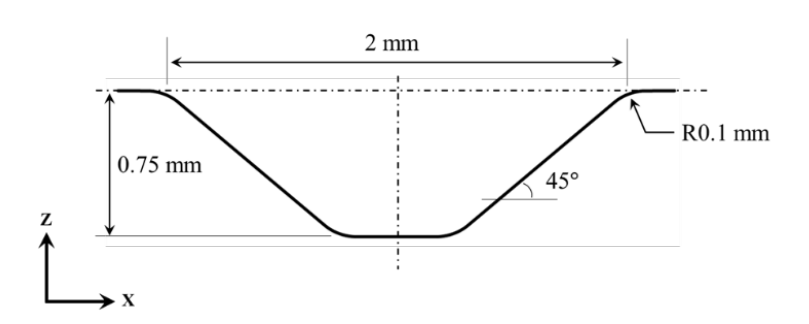


Figure 1: Baseline geometries with truncated conical shape designed for comprehensive investigation of µSPIF process

Finite Element Modeling

With the same toolpath used in experiments, a full simulation is performed in a commercial FEA software ABAQUS\Explicit. Kim et al. [14] conducted a parametric study on FE simulations of ISF process to analyze the effect of analytical and discreet rigid tool on prediction of forming forces. They observed abnormal force peaks in the predictions with discreet rigid tool due to unstable contact between coarse rigid elements of tool and the workpiece. Therefore, in this study, the tool is modeled to be analytically rigid with a hemispherical tip of 200 μ m diameter. It is expected to reduce contact noise due to smoother surface description and predict more realistic trend of reactionary forces. To imitate the experimental conditions, an initial circular workpiece of 8 mm is modeled with all six degrees of freedom constrained at its periphery to avoid any material draw. It is meshed using C3D8R elements, with five elements through-thickness, into two sections - a. one under deformation zone (which comes in contact with the tool) and b. the flange area (where tool does not contact the foil). A penalty method of contact enforcement is utilized to define contact in the tool-sheet interaction area. For this, a general-type surface-to-surface contact between top surface of the sheet and tool outer surface is defined with frictional coefficient (μ) of 0.1 to avoid any penetration of tool surface into foil material.

The material AL 1100 with 50 µm thickness is chosen for all the baseline experiments and model verification in this study since it is close to pure aluminum and known for excellent formability characteristics. Tensile tests are performed on a DMA RSA-3 of TA Instruments equipment to characterize strain hardening behavior and plastic flow curve. As a response to the experimentally obtained true plastic curves, Holloman and Voce-type strain hardening functions are chosen to demonstrate the significant difference between them. Both these strain hardening functions are mathematically represented as Equations (1) and (2), respectively. Upon extrapolation to large strain values, Holloman and Voce-type functions start to deviate from each other and might lead to erroneous prediction results. Further simulation study revealed that Holloman law yielded better prediction results therefore is utilized throughout this study with a note that further investigation in this matter would be required.

$$\bar{\sigma}(\bar{\varepsilon}^p) = K * (\bar{\varepsilon}^p)^n \tag{1}$$

$$\bar{\sigma}(\bar{\varepsilon}^p) = \sigma_Y + (\sigma_S - \sigma_Y) * \left[1 - e^{-\beta \bar{\varepsilon}^p}\right]$$
(2)

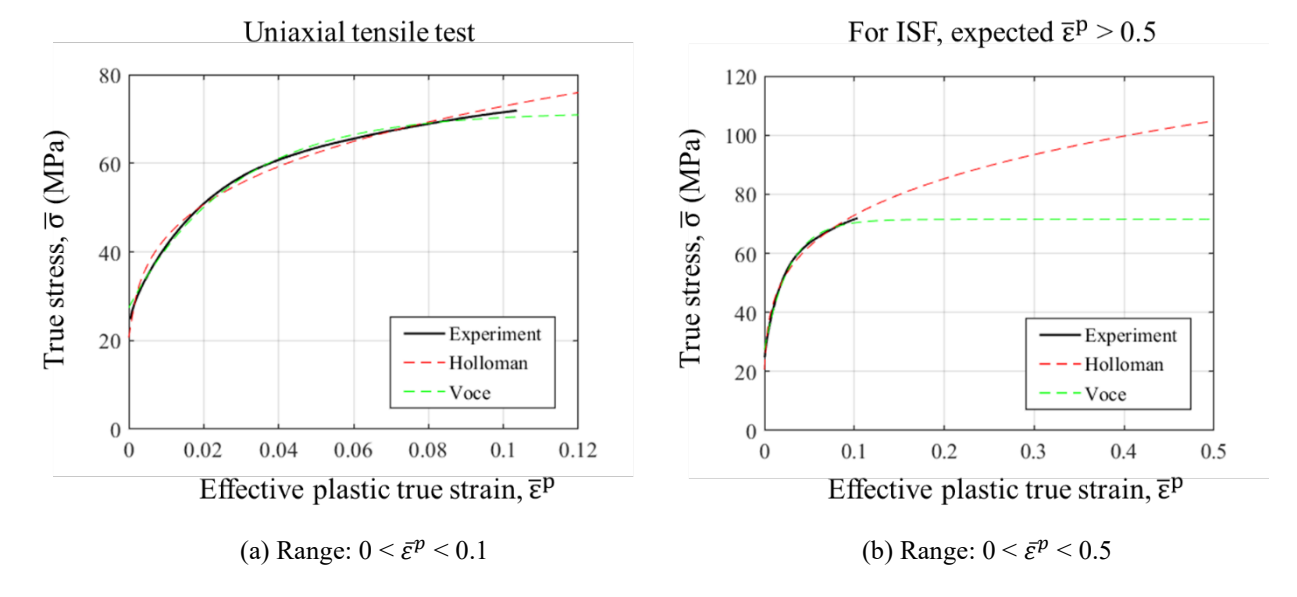


Figure 2: (a) Effective plastic stress-strain response of Al 1100 material under uniaxial tensile loading and (b) Holloman and Voce strain hardening functions fit through the experimental data and extrapolated to known ISF strains

where, $\bar{\sigma}$ and $\bar{\varepsilon}^p$ are plastic true stress and strain respectively; K = 122.6 and n = 0.226 are the strength coefficient and strain hardening exponent in Holloman law; $\sigma_Y = 27.4$, $\sigma_S = 44.1$ and $\beta = 36.08$ are initial yield stress, saturation stress and material constant in Voce-type hardening law, respectively.

Results and Discussion

It is important to develop a FE model that is computationally efficient and still provides acceptable prediction accuracy. Therefore, four different models (Case 1 to Case 4) are implemented with different FE parameters such as part meshing and mass scaling as summarized in Table 1. In all these models, five elements in through the thickness direction are used to capture any effects of high shear deformation.

Table 1: Input parameters and material properties used for benchmarking of finite element analysis

		Case 1	Case 2	Case 3	Case 4
Targeted part shape		Truncated cone shape with 45° wall angle ABAQUS\Explicit			
Material model	Hardening Law	Holloman type, isotropic	Holloman type, isotropic	Holloman type, isotropic	Holloman type, isotropic
	Yield locus	von Mises	von Mises	von Mises	von Mises
Element type		Solid element with reduced integration	Solid element with reduced integration	Shell element with reduced integration	Solid element with reduced integration and hourglass control
Mass scaling factor		1.0E7	1.0E6	1.0E6	1.0E7
Friction condition		Penalty, 0.1	Penalty, 0.1	Penalty, 0.1	Penalty, 0.1
Total # of elements		209,450 (5 in t ₀)	209,450 (5 in t ₀)	47,277	209,450 (5 in t ₀)
Number of CPUs		108	108	72	108
CPU time HH:MM:SS		40:41:47	102:00:30	77:40:15	29:38:05

Effect of mass scaling: First two cases are meshed using C3D8R 8-noded solid elements with 209,450 elements. Only mass scaling is changed and reduced by an order of magnitude in Case 2 when compared with Case 1 to study its effect on prediction accuracy and computation time. On comparing their forming forces, Case 1 results do show promising predictions when compared to the experimental results up to half depth (2200 sec) as shown in Figure 4. However, numerically obtained force values start to fluctuate after the half depth and deviate from the expected force behavior observed in experiments. When mass scaling is reduced by one order of magnitude in Case 2, the force fluctuations disappear and show good agreement with experimental values. These fluctuations can be attributed to the increase in system kinetic energies as compared in Figure 3(a). There are sudden oscillations in kinetic energy of Case 1 with M.S. = 1×10^7 after half depth of the part. This dynamic effect leads to erroneous prediction of residual stresses and consequently incorrect part geometry as previously compared. Although the prediction results are improved in Case 2, the computation time due to reduced mass scaling significantly increases from approx. 40 hours to 120 hours.

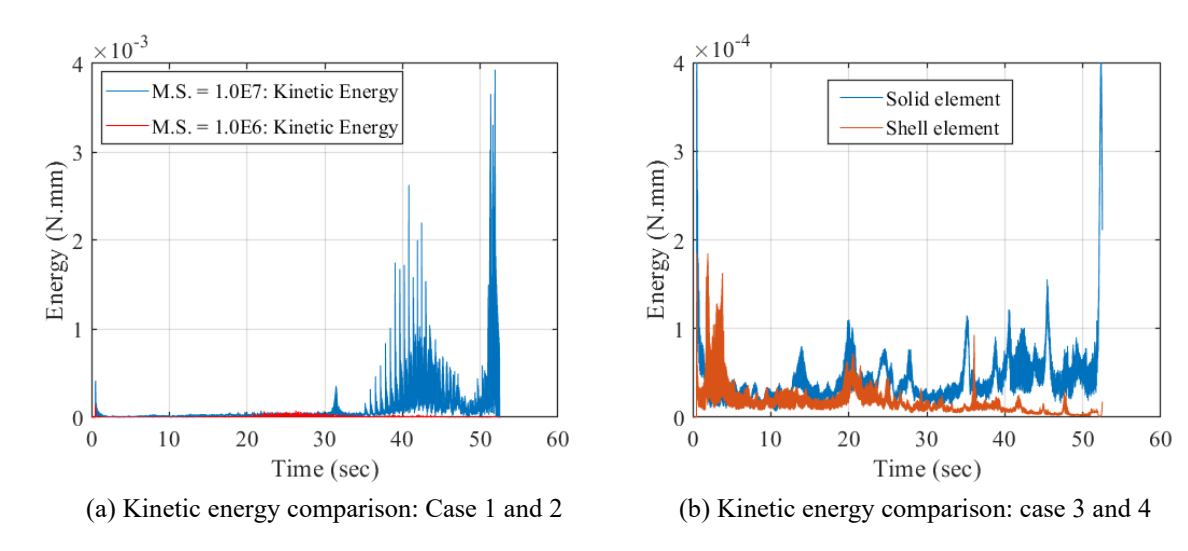


Figure 3: Comparison of kinetic energys of the simulated cone 45° part

Effect of element-type selection: Evaluating the effect of different element-type technologies in context of μSPIF process is of significant importance in terms of achieving acceptable prediction accuracy in conjunction with lowering computation costs. As previous mentioned, ISF process is known to have very high strain deformations, thousands of deformation steps and triaxial stress state which makes the computation expensive. Therefore, three different element formulations are examined in this sub-section as: (a) Solid element with reduced integration (Cases 1 and 2); (b) Shell element with reduced integration (Case 3); and (c) Solid element with reduced integration and stiffness-based hourglass control (Case 4) to analyze how it changes the nature and magnitude of reactionary forming forces.

Simulation with shell elements tends to underpredict the equivalent strain distribution. But the best deformed mesh quality is obtained in Case 4 with stiffness control formulation where no sign of "hourglassing" or excessive element distortion can be observed. This can also be confirmed by comparing their kinetic energies as in Figure 3(b). Both Cases 3 and 4 have approximately 10 times lower kinetic energy when compared with Cases 1 and 2. This demonstrates that elements with hourglass control keeps element deformation in check and does not allow dynamic effects to overtake simulation results. Furthermore, computation time in Case 4 is reduced to 29.6 hours compared to Case 1 time of 40.7 hours where all other parameters except hourglass control are kept same.

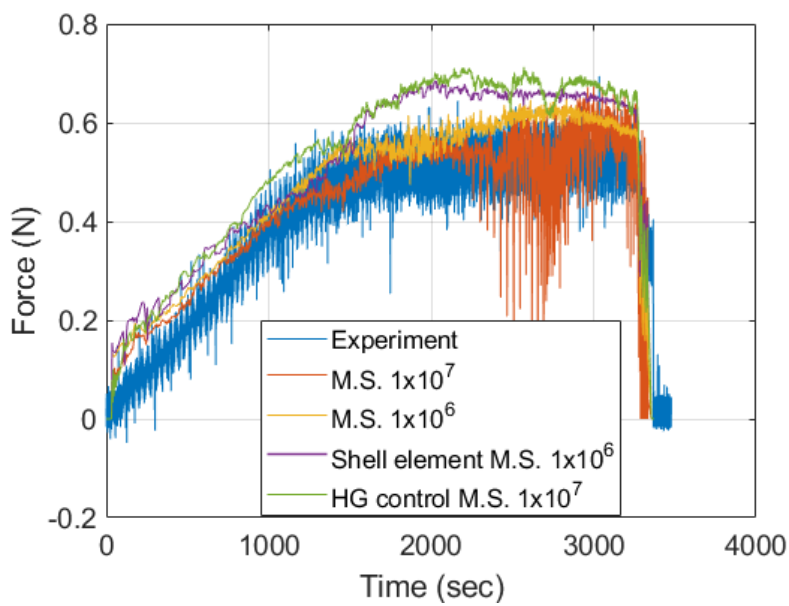


Figure 4: Comparison of experimentally obtained and FE predicted forming forces in z-direction

However, the force values predicted in both Cases 3 and 4 are slightly higher compared to Case 1 and the experimental results as shown in Figure 4. This over-prediction can be attributed to implementing the hourglassing control formulation which artificially increases the element stiffness and avoid hourglassing. Based on all the above benchmarking with cone 45° geometry, it is clearly understood that best FE prediction results can be obtained with parameters used in Case 2 simulation.

Conclusions

The main objective of this chapter was to develop a finite element prediction model for μ ISF process that does not require months of computation time and can still be very helpful in understanding the underlying process mechanics. After optimizing input parameters for the model and characterizing behavior AL 1100 under large strain deformation, some of the major take-away from this article are as follow:

- While benchmarking with cone 45° geometry, it is shown that the FE model with M.S. = 1 x 10⁶ converges best prediction results with "good enough" mesh quality. Increasing the mass scaling leads to wrinkles in the geometry due to increase in system kinetic energy and stiffness based hourglass control provides over-predicted force values.
- Multiple mass scaling factors and element types are tested in FE simulation of the above-mentioned case. Most optimum results are obtained with: (a) solid continuum element with reduced integration and (b) M.S. = 1×10^6 .

References

- [1] M. W. Fu and W. L. Chan, "A review on the state-of-the-art microforming technologies," *Int. J. Adv. Manuf. Technol.*, vol. 67, no. 9–12, pp. 2411–2437, 2013.
- [2] M. Malinauskas *et al.*, "3D Microporous Scaffolds Manufactured via Combination of Fused Filament Fabrication and Direct Laser Writing Ablation," *Micromachines*, vol. 5, no. 4, pp. 839–858, Sep. 2014.
- [3] Y. Saotome and T. Okamoto, "An in-situ incremental microforming system for three-dimensional shell structures of foil materials," *J. Mater. Process. Technol.*, vol. 113, no. 1–3, pp. 636–640, 2001.
- [4] T. Obikawa, S. Satou, and T. Hakutani, "Dieless incremental micro-forming of miniature shell objects of aluminum foils," *Int. J. Mach. Tools Manuf.*, vol. 49, no. 12–13, pp. 906–915, Oct. 2009.
- [5] T. Obikawa and M. Hayashi, "Ultrasonic-assisted incremental microforming of thin shell pyramids of metallic foil," *Micromachines*, vol. 8, no. 5, p. 142, May 2017.
- [6] Z. Xu, L. Peng, and E. Bao, "Size effect affected springback in micro/meso scale bending process: Experiments and numerical modeling," *J. Mater. Process. Technol.*, vol. 252, pp. 407–420, Feb. 2018.
- [7] L. F. Peng, Z. T. Xu, M. W. Fu, and X. M. Lai, "Forming limit of sheet metals in meso-scale plastic forming by using different failure criteria," *Int. J. Mech. Sci.*, vol. 120, pp. 190–203, Jan. 2017.
- [8] A. K. Behera, R. A. de Sousa, G. Ingarao, and V. Oleksik, "Single point incremental forming: An assessment of the progress and technology trends from 2005 to 2015," *J. Manuf. Process.*, vol. 27, pp. 37–62, Jun. 2017.
- [9] M. Bambach, "Performance Assessment of Element Formulations and Constitutive Laws for the Simulation of Incremental Sheet Forming (ISF)," 2005.

- [10] R. Esmaeilpour *et al.*, "Calibration of Barlat Yld2004-18P yield function using CPFEM and 3D RVE for the simulation of single point incremental forming (SPIF) of 7075-O aluminum sheet," *Int. J. Mech. Sci.*, vol. 145, pp. 24–41, 2018.
- [11] R. Esmaeilpour *et al.*, "Experimental validation of the simulation of single-point incremental forming of AA7075 sheet with Yld2004-18P yield function calibrated with crystal plasticity model," *Int. J. Adv. Manuf. Technol.*, pp. 1–17, Feb. 2021.
- [12] N. Moser, D. Leem, K. Ehmann, and J. Cao, "A high-fidelity simulation of double-sided incremental forming: Improving the accuracy by incorporating the effects of machine compliance," *J. Mater. Process. Tech.*, vol. 295, no. November 2020, p. 117152, 2021.
- [13] A. Bansal, B. Jiang, and J. Ni, "Die-less fabrication of miniaturized parts through single point incremental micro-forming," *J. Manuf. Process.*, vol. 43, pp. 20–25, May 2019.
- [14] H. Kim, T. Park, R. Esmaeilpour, and F. Pourboghrat, "Numerical Study of Incremental Sheet Forming Processes," *J. Phys. Conf. Ser.*, vol. 1063, no. 1, 2018.
- [15] L. Peng, X. Lai, H. J. Lee, J. H. Song, and J. Ni, "Analysis of micro/mesoscale sheet forming process with uniform size dependent material constitutive model," *Mater. Sci. Eng. A*, vol. 526, no. 1–2, pp. 93–99, 2009.
- [16] H. Wielage, Z. Hu, and F. Vollertsen, "Fracture behavior of thin foils," *J. Mater. Process. Technol.*, vol. 212, no. 3, pp. 685–688, Mar. 2012.